CrystEngComm

Photoelectrochemical epitaxy of silver oxide clathrate Ag7O8M (M= NO3, HSO4) on rutile-type Nb-doped TiO2 single crystals

Journal:	*CrystEngComm*
Manuscript ID:	CE-ART-02-2015-000329.R1
Article Type:	Paper
Date Submitted by the Author:	01-Apr-2015

Complete List of Authors:	Tanaka, Ryohei; Tokyo Institute of Technology, Materials and Structures Laboratory Takahashi, Ryota ; University of Tokyo, Institute for Solid State Physics Takata, Shintaro; Tokyo Institute of Technology, Materials and Structures Laboratory Lippmaa, Mikk; University of Tokyo, Institute for Solid State Physics Matsumoto, Yuji; Tohoku University, Applied Chemistry; Tokyo Institute of Technology, Materials and Structures Laboratory

Photoelectrochemical epitaxy of silver oxide clathrate Ag_7O_8M (M= NO_3, HSO_4) on rutile-type Nb-doped TiO_2 single crystals

Ryohei Tanaka[a], Ryota Takahashi[b], Shintaro Takata[a], Mikk Lippmaa[b], and Yuji Matsumoto[a,c]*

Received (in XXX, XXX) Xth XXXXXXXXX 20XX, Accepted Xth XXXXXXXXX 20XX
DOI: 10.1039/b000000x

Silver oxide clathrate Ag_7O_8M (M = NO_3, HSO_4) compounds were synthesized photo-electrochemically on rutile-type Nb-doped TiO_2 single-crystal substrates. Epitaxial crystal growth was achieved for some clathrate compositions and substrate surface orientations, where commensurate growth is possible due to lattice matching between the pseudo lattice of the clathrate Ag_6O_8 cages and the TiO_2 surface, similar to the well-known case of epitaxial C_{60} growth on single-crystal substrates. Particularly for the growth of $Ag_7O_8NO_3$ on Nb-doped TiO_2(110), fully (111)-oriented epitaxial crystallites without any other orientations were obtained. The selectivity for $Ag_7O_8NO_3$ growth and the suppression of the formation of by-products, such as O_2, was found to depend on the electrode potential. The highest selectivity was obtained at +0.2V vs Ag in a 0.01M $AgNO_3$ solution. An investigation of Ag_7O_8(MM') (M = NO_3, M'=HSO_4) depositions from solutions with different $AgNO_3$ and Ag_2SO_4 mixing ratios showed that the growth of $Ag_7O_8HSO_4$ is much faster than $Ag_7O_8NO_3$. The process of incorporating monovalent M anions into the clathrate Ag_6O_8 cages was identified as the rate-limiting step for the growth of silver oxide clathrate compounds.

1. Introduction

Silver oxide clathrates with a general formula of Ag_7O_8M are a class of clathrate compounds where M is a monovalent molecular anion that is surrounded by Ag_6O_8 cages[1]. Possible molecular anions in silver oxide clathrates include NO_3, HSO_4, ClO_4, HF_2, BF_4, PF_6, and HCO_3 [2-4], with some of the compounds exhibiting superconductivity at low temperatures, such as $Ag_7O_8NO_3$ that has a *T*c of 1.04 K[5, 6]. As is evident from the chemical formula, a Ag_6O_8 cage contains Ag ions in multiple valence states, including Ag^+, Ag^{2+}, and Ag^{3+}. Silver oxide clathrate compounds can therefore be synthesized only under strongly oxidizing conditions and, as a result, they are thermodynamically unstable and likely to undergo self-decomposition into AgO_x and other derivatives in air even at room temperature[7].

So far, several different methods of synthesizing Ag_7O_8M have been reported, but depending on the concentration of Ag^+, the pH, and the choice of the counter anion, most methods lead to the formation of various simple binary silver oxides, such as Ag_3O_4, Ag_2O_4, Ag_2O or Ag_2O_2 in addition to the desired clathrate phase[7-11]. Electrochemical oxidation in a 5M $AgNO_3$ aqueous solution with pH=1.45 is usually preferred for the synthesis of $Ag_7O_8NO_3$, using a Pt electrode that is biased beyond the $Ag_7O_8NO_3$ equilibrium potential of +1.59V vs the standard hydrogen electrode potential (SHE)[9]. We have shown earlier that $Ag_7O_8NO_3$ films can be synthesized photocatalytically under ultraviolet (UV) light irradiation in an aqueous $AgNO_3$ solution either directly on Nb- or La-doped $SrTiO_3$(001) single crystals[12]. $Ag_7O_8NO_3$ is metallic among many photo-oxidized products, and thus the photo-deposition process of $Ag_7O_8NO_3$ on substrates that have been coated with an epitaxial ferroelectric $PbTiO_3$ thin film can be used for an efficient domain switching to pole a large area because the metallic $Ag_7O_8NO_3$ simultaneously photo-deposited is able to stabilize the resultant polar surface[13, 14, 15], as one of the possible applications. A common feature of all these surfaces is the presence of valence band levels that are derived predominantly from O2*p* states and are thus more positive than the equilibrium potential. Similar light-induced deposition of $Ag_7O_8NO_3$, though not photocatalytically, has been observed on GaAs substrates when synchrotron X-rays were used as a light source[16]. More recently, we also demonstrated photoelectrochemical synthesis of $Ag_7O_8NO_3$ on Nb-doped $SrTiO_3$(001) single-crystal electrodes in a $AgNO_3$ solution and discussed the role of the electrode potential in this photochemical process[17].

Despite the availability of different synthesis methods, the crystal growth mechanism of silver oxide clathrate compounds is still very poorly understood. In particular, it is not clear if silver oxide clathrates can be epitaxially grown on appropriate lattice-matched single-crystal substrates. There is a growing interest in developing electrochemical room-temperature epitaxy techniques, often termed "electrochemical epitaxy" [18]. However, the growth of silver oxide clathrate compounds is usually not epitaxial, even when single-crystal electrodes, like Pt(100), Pt(111), Pt(110)[10] or Nb-doped $SrTiO_3$(001) are used, probably due to the large difference in the crystal structures of the clathrate films and the single-crystal substrate electrodes. So far, only out-of-plane orientation control has been achieved in the growth of $Ag_7O_8NO_3$ onto Pb-Tl-O buffer layers[11] but there is no

conclusive data on epitaxial growth of any silver oxide clathrate compounds. If epitaxy for these materials can be achieved, a new guiding principle may be developed for epitaxial growth of materials that have very different crystal structures from the substrate.

In the present work, we therefore examine the possibility of epitaxial photoelectrochemical growth of $Ag_7O_8NO_3$ and $Ag_7O_8HSO_4$ on Nb-doped TiO_2 single crystals under UV irradiation at a well-controlled electrode potential and compare the results with earlier studies that used Nb-doped $SrTiO_3(001)$ as a substrate. Since the clathrate formation reaction competes with water photo-oxidation, we take a careful look at the electrode potential dependence of the reaction selectivity against the formation of byproducts, such as O_2. The crystal growth mechanism of silver oxide clathrates is studied by investigating the growth behaviour of $Ag_7O_8(MM')$ (M = NO_3, M'=HSO_4) in mixtures of $AgNO_3$ and Ag_2SO_4 solutions at different mixing ratios. We identify the rate-limiting step for the growth of silver oxide Ag_7O_8M clathrate compounds and show that single-phase $Ag_7O_8NO_3$ can be epitaxially grown on Nb-doped $TiO_2(110)$ surfaces.

2. Experimental Section

We used single-crystal *n*-type 0.5 wt% Nb-doped rutile TiO_2 substrates with (110), (101), (100), and (001) surface cuts from Shinkosha[19]. Ohmic substrate contacts were made by coating the backside of the crystals with an In-Ga alloy and attaching copper wires with silver paste. All parts of the samples, except for the middle part of the front surface, were covered with epoxy resin to avoid leak currents in the electrochemical cell. The photoelectrochemical synthesis was performed at room temperature in a three-electrode electrochemical cell, using a Pt plate counter electrode and a silver wire reference electrode. The electrolytes used in this study included 0.01M $AgNO_3$ and 0.01M Ag_2SO_4 aqueous solutions, and mixtures of $AgNO_3$ and Ag_2SO_4 solutions with different mixing ratios. The photoelectrochemical reaction was carried out under UV light illumination from a high-pressure Hg lamp (Ushio, USH-150SC) at a constant flux of 28 mW/cm^2 and the photocurrent was recorded at a sampling rate of 5 Hz. The light intensity was measured with an integrating light counter for 254 nm (Ushio, UIT-150-A). The electrode potential was set in the range between −0.5 and +1 V vs Ag. After photoelectrochemical treatment, the deposited materials were first identified by θ-2θ X-ray diffraction (XRD) analysis (MAC Science SRA M18XHF22), followed by, if needed, X-ray Φ scan analysis (PANalytical X'Pert PRO MRD) in order to investigate the epitaxial in-plane orientation of the $Ag_7O_8NO_3$ and $Ag_7O_8HSO_4$ crystals with respect to the TiO_2 substrate lattice. The morphology of the $Ag_7O_8NO_3$ and $Ag_7O_8HSO_4$ crystals was observed by scanning electron microscopy (SEM) and electron probe microanalysis (EPMA) was used to estimate the total volume and the composition of the deposition products (Hitachi S-4000). The photocatalytic reaction kinetics on Nb-doped TiO_2 was investigated by measuring the relative selectivity σ between $Ag_7O_8NO_3$ and other byproducts, such as O_2. The selectivity is defined as

$$\sigma = \frac{I(Ag/Ti)}{Q_{photo}} \quad (1)$$

where *I*(Ag/Ti) is the measured EPMA intensity ratio of Ag and Ti, and Q_{photo} is the total electrical charge conveyed per unit surface area by the photocurrent during the photoelectrochemical reaction.

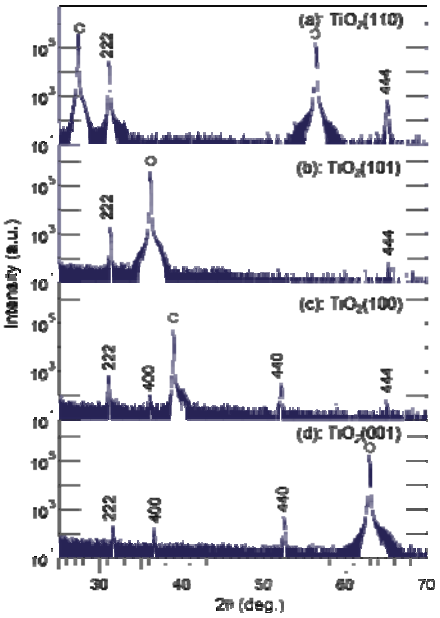

Figure 1. A set of θ-2θ XRD patterns of photoelectrochemically deposited $Ag_7O_8NO_3$ on Nb-doped TiO_2(110), (101), (100), and (001) single-crystal substrates in a 0.01M $AgNO_3$ solution at an electrode potential of +0.3 V vs Ag. The deposition time was 2 h. All plots are shown on a logarithmic scale .

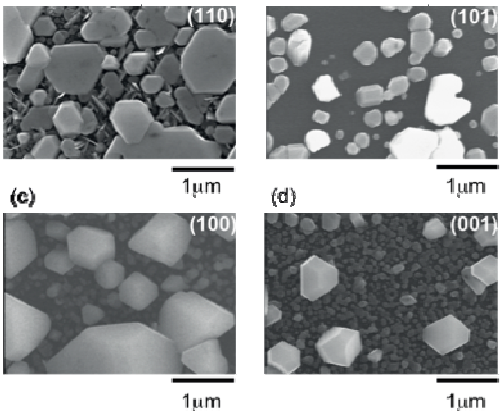

Figure 2. SEM images of the same set of $Ag_7O_8NO_3$ samples that were used for the XRD analysis in Fig. 1.

3. Results and discussion

3. Results and discussion

3.1. Growth of $Ag_7O_8NO_3$ on Nb-doped TiO_2 single crystals.

Figure 1 shows θ-2θ XRD patterns of $Ag_7O_8NO_3$ crystals that were photoelectrochemically deposited in 2 hours on Nb-doped TiO_2 (110), (101), (100), and (001) single-crystal substrates in

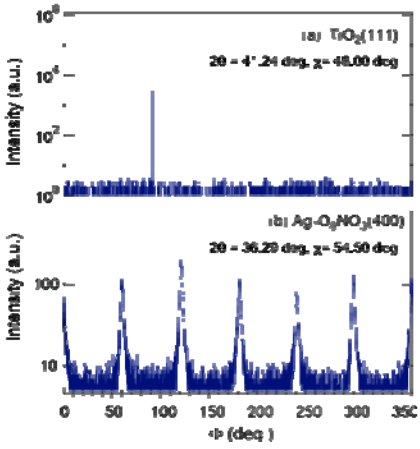

Figure 3. X-ray Φ scans of the TiO_2(111) and $Ag_7O_8NO_3$(400) reflections for a (111)-oriented $Ag_7O_8NO_3$ sample epitaxially grown on a TiO_2(110) substrate. Six clathrate peaks were observed from two equivalent domains rotated by 180° relative to each other.

0.01M $AgNO_3$ at an electrode potential of +0.3V vs Ag. Diffraction peaks were observed at 2θ=31.28°, 36.27°, 52.26°, and 65.56° [20], revealing that only $Ag_7O_8NO_3$ was deposited on the TiO_2 substrates, irrespective of the crystal face. No other peaks that could be assigned to binary silver oxides were detected. All XRD patterns in Fig. 1 show reflections of (111)-oriented $Ag_7O_8NO_3$ crystals. In particular, Fig. 1(a) shows that the 222 peak for the sample grown on TiO_2(110) has the highest intensity, even though the deposition time is identical. As the FWHM values for the θ–2θ scans are not so different, the highest intensity of $Ag_7O_8NO_3$ on the TiO_2(110) is due to its unique out-of-plane orientation.

The crystal quality of $Ag_7O_8NO_3$ was further analyzed by visualizing the grain structure by SEM, as shown in Fig. 2. It is clear that a few large faceted crystals and many small grains grew on TiO_2(101), (100), and (001) substrates, suggestive of a polycrystalline nature of $Ag_7O_8NO_3$ on these surfaces. Only Fig. 2(a) shows large hexagonal crystal platelets with a unique in-plane orientation growing on a TiO_2(110) substrate. This implies epitaxial growth of (111)-oriented $Ag_7O_8NO_3$ crystals on the TiO_2(110) substrate. The thickness for each $Ag_7O_8NO_3$ platelet could be estimated to be in a range of a few hundred nanometers from the cross-sectional SEM image (not-shown). The epitaxial relationship was determined from Φ scans recorded for the TiO_2(111) and $Ag_7O_8NO_3$(400) reflections, as shown in Fig. 3. There are six $Ag_7O_8NO_3$(400) peaks and two TiO_2(111) reflection peaks, which means that (111)-oriented $Ag_7O_8NO_3$ grew epitaxially on TiO_2(110) in two equivalent domains that are rotated by 180° with respect to each other. The in-plane relationship between the $Ag_7O_8NO_3$ crystals and the TiO_2(110) substrate is

$$Ag_7O_8NO_3(111)[1\bar{1}0]//TiO_2(110)[001],$$
$$Ag_7O_8NO_3(111)[11\bar{2}]//TiO_2(110)[1\bar{1}0]$$
or
$$Ag_7O_8NO_3(111)[11\bar{2}]//TiO_2(110)[1\bar{1}0].$$

The FWHM value of the (111)-oriented epitaxial $Ag_7O_8NO_3$ film on TiO_2(110), estimated from the Φ scan, is as large as 1.815 deg., suggesting that the crystallinity and mosaic spread, though

Table 1

Epitaxial relationship between TiO_2 substrates and $Ag_7O_8NO_3$ crystals.

Substrate	$Ag_7O_8NO_3$ epitaxial orientation	$Ag_7O_8NO_3$ non-epitaxial orientation	$Ag_7O_8NO_3$ in-plane direction	[0] in-plane direction
[illegible]	(111)		[112]	[1-10]
			[11$\bar{2}$]	[001]
[illegible]	(100)	(1 0 0)	[001]	[1-10]
			[00$\bar{1}$]	[1-10]
[illegible]	(110)	(1 1 0)	[001]	[001]
		(1 1 0)	[11$\bar{2}$]	[1-10]
[illegible]	(110)	(1 1 0)	[001]	[001]
		(1 1 0)	[11$\bar{2}$]	[1-10]

these two parameters cannot be independently discussed here, should not be so excellent for the in-plane direction. Nevertheless, the X-ray analysis result is consistent with the SEM observation of a unique in-plane orientation of the large crystallites in Figs. 2(b-d). The analysis of Φ scan data, summarized in Table 1, revealed that some $Ag_7O_8NO_3$ crystals grew epitaxially on other TiO_2 crystal planes as well. For example, the data in Fig. 1 shows that (111)-oriented $Ag_7O_8NO_3$ crystals were always present, regardless of the TiO_2 substrate orientation. These photoelectrochemical deposition results are consistent with our earlier work on electrochemical deposition of

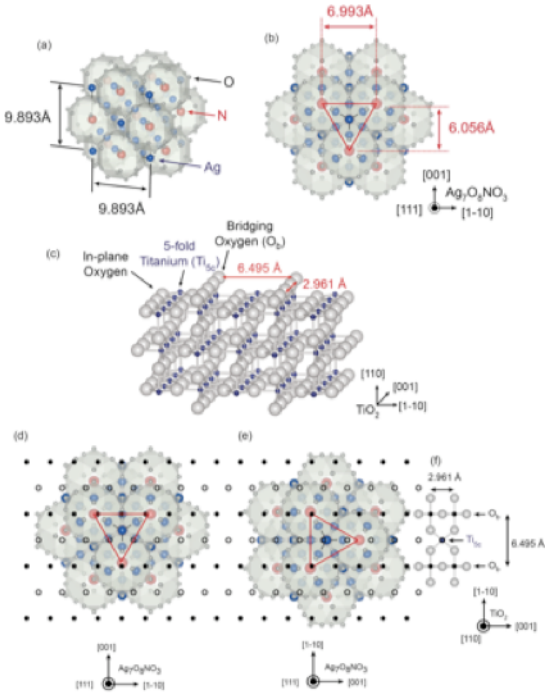

Figure 4. (a) Schematic illustration of the $Ag_7O_8NO_3$ crystal structure in a cubic system. Blue, red, and gray spheres denote Ag, N, and O, respectively. (b) A view of the (111) surface of a $Ag_7O_8NO_3$ crystal. The red lines mark the outlines of the surface unit cell of the rhombicuboctahedral pseudo lattice. (c) Illustration of the TiO_2(110) surface structure. The surface layer consists of bridging oxygens (O_b), 5-fold coordinated titanium atoms (Ti_{5c}), and in-plane oxygens. (d,e) Two possible in-plane alignments of $Ag_7O_8NO_3$ crystals on a TiO_2(110) surface. The black open and closed circles mark the positions of the Ti_{5c} and bridging titanium sites, respectively, on the underlying TiO_2(110) surface. The configuration in (d) corresponds to the experimental results in Fig. 3, showing only a small lattice mismatch between the rhombicuboctahedral cage lattice and the bridging oxygens on the TiO_2(110) surface.

clathrates on Nb:$SrTiO_3$(001) substrates[12], photodeposition on Nb- or La-doped $SrTiO_3$(001)[17], and on $PbTiO_3$/Nb:$SrTiO_3$(001)[13-15]. $Ag_7O_8NO_3$ appears to have a crystal habit of preferentially growing along the (111) direction, but the selectivity for pure (111)-oriented growth is the highest for photoelectrochemical deposition on TiO_2(110) substrates.

3.2. Epitaxial growth model of $Ag_7O_8NO_3$/Nb-doped TiO_2 interfaces.

We follow earlier work by Breyfogle et al.[11], who found that the growth orientation of $Ag_7O_8NO_3$ crystals is tuneable by selecting a suitable lattice-matched and textured Pb-Tl-O bottom layer, and consider the lattice mismatch between $Ag_7O_8NO_3$ crystals and the TiO_2 substrates. Fig. 4(a) schematically illustrates the $Ag_7O_8NO_3$ crystal structure[1], showing a network composed of large face-sharing rhombicuboctahedral Ag_6O_8 cages. Silver ions are located at the centre points of the shared cage faces and in the middle of the small cubic voids in between the cages. As is illustrated in Fig. 4(b), the dominant factor for determining whether commensurate epitaxial $Ag_7O_8NO_3$ crystal growth can occur on a substrate is the Ag_6O_8 cage size, which determines the lattice mismatch between the TiO_2 surface and the clathrate cage pseudo lattice. This is analogous to the epitaxial growth of C_{60}, which is another well-known molecular cage compound that can be epitaxially grown on single-crystal substrates[21,22]. The in-plane distances of the cage pseudo lattice viewed along the (111) direction are 6.993 Å and 6.056 Å. We have taken a closer look at the structure of the unreconstructed TiO_2(110) surface to understand the reason for the epitaxial growth of (111)-oriented $Ag_7O_8NO_3$ crystals on TiO_2(110) substrates. This surface consists of 5-fold coordinated titanium (Ti5c) atoms, in-plane oxygen atoms, and bridging oxygen atoms (Ob), as shown in Fig. 4(c). The bridging oxygen atoms are known to have a strong effect on chemical reaction at the interface between the TiO_2(110) surface and an electrolyte[23]. The distance between adjacent bridging oxygen lines is 6.495 Å. Figs. 4(d) and 4(e) show two possible in-plane alignments of (111)-oriented $Ag_7O_8NO_3$ crystals on the TiO_2(110) surface. The black closed and open circles mark the positions of Ti atoms along the Ob rows and at the Ti5c sites, respectively, as illustrated in Fig. 4(f). The model in Fig. 4(d) clearly shows a smaller lattice mismatch than that of Fig. 4(e), and corresponds to the experimentally observed in-plane orientation as shown by the Φ scan in Fig. 3. In general, it is difficult to stabilize a triangular lattice, such as that of (111)-oriented $Ag_7O_8NO_3$ crystals, on a rectangular lattice. However, the tetragonal TiO_2(110) surface has strong in-plane anisotropy, allowing the (111)-oriented $Ag_7O_8NO_3$ crystals to grow epitaxially with only moderate in-plane mismatch.

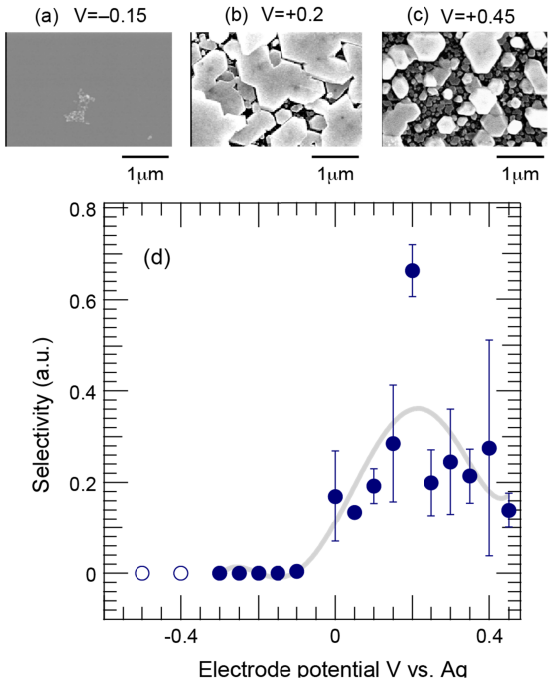

Figure 5. Relative selectivity of the formation of $Ag_7O_8NO_3$ (filled circles) as a function of electrode potential, together with SEM images taken for samples grown at electrode potentials of -0.15, +0.2 and +0.45V, respectively. Open circles correspond to the formation of Ag metal particles.

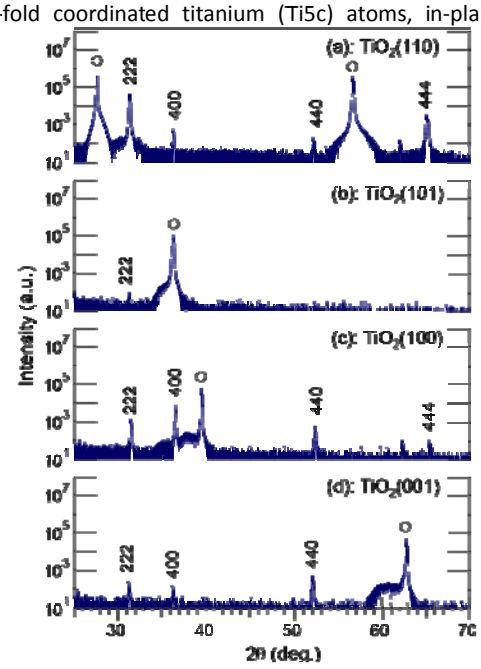

Figure 6. A set of $\theta - 2\theta$ XRD patterns of photoelectrochemically deposited $Ag_7O_8HSO_4$ samples grown on (110), (101), (100), and (001) oriented Nb-doped TiO_2 substrates. Thee crystals were grown in a 0.01M $Ag_7O_8HSO_4$ solution at an electrode potential of +0.3V vs Ag in 2 h. All plots are shown on a logarithmic scale.

3.3. Reaction selectivity against O_2 by-products.

The effect of the electrode potential on the growth of $Ag_7O_8NO_3$ crystals on TiO_2(110) was investigated. Fig. 5 shows the relative selectivity for the formation of $Ag_7O_8NO_3$ (filled circles) as a function of electrode potential, together with SEM images of crystals grown at electrode potentials of –0.15, +0.2, and +0.45 V. In principle, no deposition of $Ag_7O_8NO_3$ (*relative selectivity* = 0) should occur at negative electrode potentials vs. Ag and, as expected, the inset SEM image for the –0.15 V sample shows almost no growth. It is thermodynamically more likely for Ag ions to be reduced to Ag metal at negative electrode potentials and this behaviour was experimentally observed for electrode potentials < –0.3V, with Ag metal deposits growing on

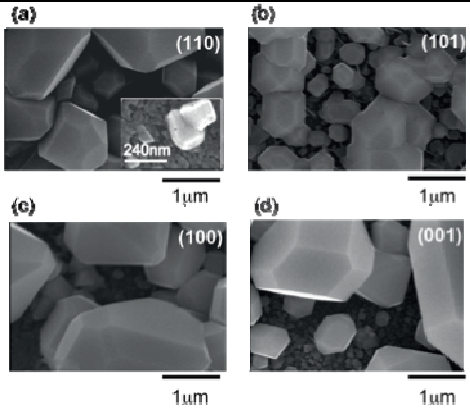

Figure 7. SEM images of $Ag_7O_8HSO_4$ crystals that were used in the XRD analysis shown in Fig. 6.

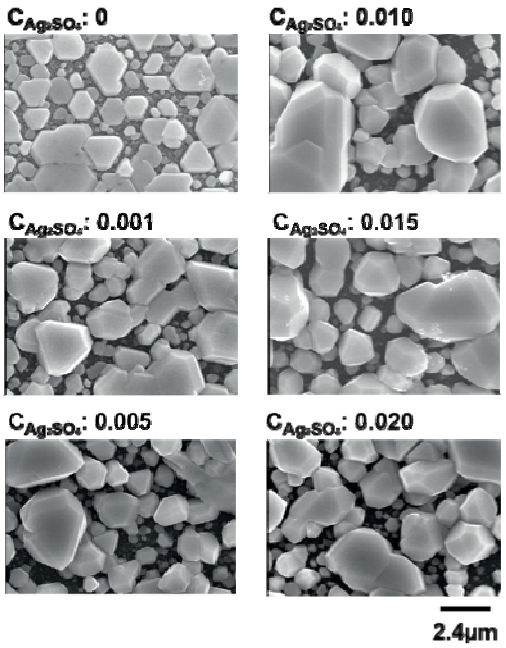

Figure 8. A series of SEM images of silver oxide clathrates compounds photodeposited in solutions of $AgNO_3$ and Ag_2SO_4 with different mixing ratios at an electrode potential of +0.3V vs Ag in 1 h.

the TiO_2 electrode instead of a clathrate phase. These data points are marked with open circles in Fig. 5. On the other hand, for positive electrode potentials, a gradual increase in the selectivity was found up to a potential of ca. +0.2 V, at which point the selectivity reached a maximum and decreased again for higher potentials. The inset SEM images of the +0.2 V and +0.45 V samples show that the selectivity changes are clearly reflected in the morphology of the crystals. Based on our earlier work on the growth selectivity of $Ag_7O_8NO_3$ on Nb-doped $SrTiO_3(001)$[17], it appears that the selectivity maximum at around +0.2 V is a common feature for silver oxide clathrates. A notable difference, however, is that on $SrTiO_3(001)$ substrates, the clathrate formation selectivity actually increased at negative electrode potentials vs. Ag, although the absolute amount of deposited $Ag_7O_8NO_3$, of course, dropped in accordance with the decreasing total photocurrent. A strong electric field, on the order of 1 MV/cm, has been shown to occur at the interface between an electrode and an electrolyte[24]. Hot carriers that can be injected through quantized interface levels due to the strong electric fields[25] may be partly responsible for the observed electrode potential dependence.

3.4. Comparison of the growth behaviours of $Ag_7O_8NO_3$ and $Ag_7O_8HSO_4$ on Nb-doped TiO_2 single crystals.

Photoelectrochemical synthesis of other types of silver oxide clathrates on Nb-doped TiO_2 single crystals was also studied under experimental conditions that were identical except for the composition of the electrolyte. $Ag_7O_8HSO_4$ crystals were successfully obtained in a 0.01M Ag_2SO_4 solution, while the synthesis of $Ag_7O_8ClO_4$ in a 0.01M $AgClO_4$ solution was possible, but the absolute amount was too small to be fully characterized. We therefore compare the growth of $Ag_7O_8HSO_4$ with $Ag_7O_8NO_3$. Figure 6 shows a set of θ – 2θ XRD patterns of $Ag_7O_8HSO_4$ layers that were photoelectrochemically deposited in 2 hours on Nb-doped TiO_2 (110), (101), (100), and (001) single-crystal substrates in 0.01M Ag_2SO_4 at an electrode potential of +0.3V vs Ag. The diffraction peak positions very close to those of $Ag_7O_8NO_3$ because of the similar lattice constants ($Ag_7O_8NO_3$: 0.989nm, $Ag_7O_8HSO_4$: 0.992nm)[7]. No other peaks belonging to binary silver oxides or any other secondary phases could be detected. According to a Φ scan analysis (not shown), some $Ag_7O_8HSO_4$ crystals always grew epitaxially, regardless of the TiO_2 substrate orientation. The relative intensities of the $Ag_7O_8HSO_4$ XRD peaks were different from those of $Ag_7O_8NO_3$, which reflects a different out-of-plane orientation preference. The main difference was the presence of (100)-oriented grains in addition to the (111)-orientation, even on TiO_2(110). A set of SEM images corresponding to the different substrate orientations is shown in Fig. 7. A comparison with the SEM images of $Ag_7O_8NO_3$ crystals in Fig. 2 clearly shows that the size and areal density of

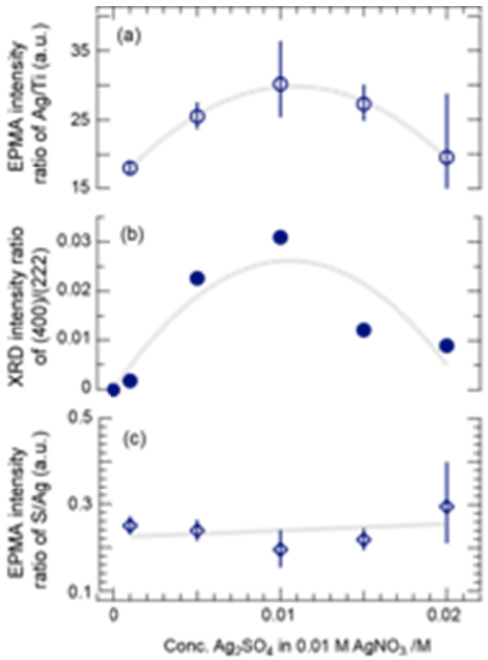

Figure 9. (a) EPMA intensity ratio of Ag/Ti as a function of the Ag_2SO_4 concentration in the photodeposition solution. The Ag/Ti ratio is proportional to the total amount of photodeposited silver oxide clathrate compounds. (b) Intensity ratio of the (400) and (222) XRD peaks. (c) EPMA S/Ag intensity ratio as a function of $c_{Ag_2SO_4}$.

$Ag_7O_8HSO_4$ crystals is considerably larger than for $Ag_7O_8NO_3$ on all TiO_2 crystal faces, but most remarkably on TiO_2(110). However, it should be pointed out that since the concentration of Ag^+ ions in a 0.01M Ag_2SO_4 solution is two times higher than in a 0.01M $AgNO_3$ solution, the growth behaviours of $Ag_7O_8NO_3$ and $Ag_7O_8HSO_4$ cannot be directly compared based on two independent experiments if the growth rate depends on the concentration of Ag^+ in the solution.

In order to rule out this possibility, simultaneous photodeposition of Ag_7O_8(MM') (M = NO_3, M'=HSO_4) onto TiO_2(110) was tested by using mixtures of $AgNO_3$ and Ag_2SO_4 solutions with different mixing ratios at an electrode potential of +0.3V vs Ag, where any unexpected effects that would appear even when all the experimental conditions are equal will be minimized. As shown by the series of SEM images in Fig. 8, no large crystallites were formed in a pure 0.01M $AgNO_3$ solution after a 2-hour deposition. As the concentration of Ag_2SO_4, c_{Ag2SO4}, in the mixed solution was increased, the number of large crystals also increased, reaching a maximum size for c_{Ag2SO4} = 0.01 and decreasing for higher Ag_2SO_4 concentrations. It is noted that a very small, e.g. 20% increase of Ag^+ in the solution by adding Ag_2SO_4 (c_{Ag2SO4} is 0.001M) is enough to cause a big change in morphology and growth rate of the silver oxide clathrates compounds. According to our previous work, the concentration dependence of the growth rate and morphology is not so strong in photocatalytic synthesis of $Ag_7O_8NO_3$ on Nb:$SrTiO_3$(001)[12], the observed changes may not be simply due to the Ag^+ concentration effect. As most of the volume of the deposited clathrate is contained in the large crystallites, the areal density of such crystals and their volume as a function of c_{Ag2SO4} should be proportional to the total amount of photodeposited silver-oxide clathrate compounds, which can be measured from the EPMA Ag/Ti intensity ratio as shown in Fig. 9(a). On the other hand, the intensity ratio of the 400 and 222 XRD peaks, plotted as a function of c_{Ag2SO4} in Fig. 9(b), shows a similar tendency as the Ag/Ti intensity ratio. The large crystals can thus be identified as being (100)-oriented clathrate crystals. The large number of smaller plate-like crystals that can be seen in the inset of Fig. 7(a) are spread under and around the large (100) crystals and appear to have formed at the initial growth stage. These small crystallites are responsible for the weaker 222 and 444 XRD peaks in Fig. 6 and these crystallites are thus oriented along the (111) direction. As was pointed out earlier, among the silver oxide clathrates studied here, only $Ag_7O_8HSO_4$ crystals can grow along the (100) direction on TiO_2(110). We can therefore conclude that when mixtures of $AgNO_3$ and Ag_2SO_4 solutions are used under the present experimental conditions, the dominant (100)-oriented Ag_7O_8(MM') phase is either pure $Ag_7O_8HSO_4$ or at least a $Ag_7O_8HSO_4$–rich mixed clathrate. The preferential formation of $Ag_7O_8HSO_4$ clathrate is probably caused by the faster growth rate of $Ag_7O_8HSO_4$ crystals when compared to $Ag_7O_8NO_3$ for both (100) and (111) orientations. As can be seen in the inset of Fig. 7(a), the average size of the (111)-oriented crystals of $Ag_7O_8HSO_4$ is much smaller than for the $Ag_7O_8NO_3$ crystals in Fig. 2(a). Both images were taken after a 2-hour photodeposition run under otherwise identical conditions. This size difference can be understood in terms of the kinetic effect, i.e., a higher growth rate leads to the formation of a larger number of smaller crystals. The small (111)-oriented crystallites grown from a mixed solution may contain $Ag_7O_8NO_3$ or $Ag_7O_8NO_3$-rich mixed clathrates as well as $Ag_7O_8HSO_4$, but the volume fraction of the former must be very small due to the lower growth rate. This assumption is supported by the observation that, as shown in Fig. 9(c), the EPMA intensity ratio of S to Ag appears to be nearly constant, irrespective of the mixing ratio of the growth solution. Furthermore, the decrease of the EPMA Ag/Ti intensity ratio, i.e., the amount of $Ag_7O_8HSO_4$ or $Ag_7O_8HSO_4$–rich mixed clathrates deposited as a major product, at higher c_{Ag2SO4} than 0.01M can be understood when considering the very narrow Ag^+ ion concentration window of less than 0.005M where $Ag_7O_8HSO_4$ can be synthesized by electrochemical oxidation[2].

In simultaneous photodeposition of Ag_7O_8(MM') (M = NO_3, M'=HSO_4) the process that forms Ag_6O_8 cages through the oxidation of Ag^+ ions is common for both materials and the rate-limiting step for the growth of silver oxide clathrate Ag_7O_8M compounds must therefore be a process that involves the monovalent anions. It is possible, for example, that different incorporation kinetics of the anions inside the Ag_6O_8 cages is responsible for the observed differences in the $Ag_7O_8NO_3$ and $Ag_7O_8HSO_4$ growth rates.

4. Conclusion

We have succeeded in photoelectrochemical synthesis of silver oxide clathrate Ag_7O_8M (M= NO_3, HSO_4) compounds on Nb-doped rutile TiO_2 single-crystal substrates. An epitaxial relationship between clathrate crystals and TiO_2 substrates was found for some combinations of the clathrate anions and substrate orientations, with a particularly clear case being the fully (111)-oriented growth of $Ag_7O_8NO_3$ occurring on TiO_2(110). This result has confirmed that commensurate, epitaxial lattice matching can occur between a single-crystal substrate lattice and the pseudo lattice of cages in an inorganic compound, such as the $Ag_7O_8NO_3$ clathrate used in this work. This work shows that such matching is not unique to organic cage compounds like C_{60}. A certain electrode potential of ca. +0.2 V vs Ag resulted in preferential deposition of $Ag_7O_8NO_3$ over other by-products. It was found that the process of incorporating monovalent anions, such as NO_3^- or HSO_4^- into the Ag_6O_8 cages is a possible rate-limiting step in this photoelectrochemical silver oxide clathrate synthesis, leading to different growth rates of $Ag_7O_8NO_3$ and $Ag_7O_8HSO_4$.

Acknowledgement

This work was partially supported by Grant-in-Aid from the Ministry of Education, Culture, Sports, Science and Technology of Japan (Nos. 20360294, 25706022, 26105002) and the Asahi Glass Foundation. Some of experiments were performed using the joint-use facilities of the Institute for Solid State Physics, the University of Tokyo. Crystal structure illustrations were generated with VESTA[26].

Notes and references

[a] *Materials and Structures Laboratory, Tokyo Institute of Technology,*

4259 Nagatsuta, Midori-ku, Yokohama 226-8503 Japan.
[b] Institute for Solid State Physics, University of Tokyo, 5-1-5 Kashiwanoha, Kashiwa, Chiba 277-8581, Japan,
[c] Department of Applied Chemistry, School of Engineering, Tohoku University*
6-6-07 Aramaki Aza Aoba, Aoba-ku Sendai,980-8579 Japan
Tel: 081-22-795-7266, Fax: 081-22-795-7268,
E-mail: matsumoto@atomol.che.tohoku.ac.jp

1. I. Náray-Szabó, G. Argay, and P. Szabó, *Acta Crystallogr.* 1965, **19**, 180–184.
2. B. Standke, and M. Jansen, *J. Solid State Chem*. 1987, **67**, 278–284.
3. A. Parkin, S. F. Johnstone, A. R. Mount, S. Parsons, C. R. Pulham, and D. Sanders, , *J. Appl. Cryst.* 2004, **37**, 312–318.
4. M. Jansen, and S. Vensky, *Z Naturfosch. B* 2000, **55**, 882–886.
5. M. B. Robin, K. Andres, T. H. Geballe, N. A. Kuebler, and D. B. McWhan, *Phys. Rev. Lett*. 1996, **17**, 917–919.
6. K. Kawashima, M. Ishii, H. Okabe, J. Akimitsu, M. Kriener, H. Takatsu, S. Yonezawa, and Y. Maeno, *J. Phys. Soc. Jpn.* 2008, **77**, 024707(1-5).
7. G. I.N. Waterhouse, J. B. Metson, and G. A. Bowmaker, *Polyhedron*, 2007, **26**, 3310–3322.
8. C. H. Wong, T. H. Lu, C. N. Chen, and T. J. Lee, *J. Inorg. Nucl. Chem.* 1972, **34**, 3253–3257.
9. S. S.Djokic, *J. Electrochem. Soc.*, 2004, **151**, C359–364.
10. E. Michailova, and A. Milchev, *J. Appl. Electro. Chem*., 1988, **18**, 614–618.
11. B. E. Breyfogle, R. J. Phillips, and J. A. Switzer, *Chem. Mater.*, 1992, **4**, 1356–1360.
12. R. Tanaka, S. Takata, M. Katayama, R. Takahashi, J. K. Grepstad, T. Tybell, and Y. Matsumoto, *J. Electrochem*., 2010, **157**, E181–183.
13. R. Takahashi, J. K. Grepstad, T. Tybell, and Y. Matsumoto, *Appl. Phys. Lett.*, 2008, **92**, 112901 (1-3)
14. R. Takahashi, M. Katayama, Ø. Dahl, J. K. Grepstad, Y. Matsumoto and T. Tybell, *Appl. Phys. Lett.*, 2009, **94**, 232901 (1-3).
15. R. Takahashi, M. Katayama, Ø. Dahl, J. K. Grepstad, Y. Matsumoto and T. Tybell, *Appl. Phys. Lett.*, 2010, **97**, 059903 (1).
16. Y. Sun, Y. Ren, D. R. Haeffner, J. D. Almer, J. D. Wang, W. Yang, and T. T. Truong, *Nano. Lett.*, 2010, **10**, 3747-3753.
17. R. Tanaka, S. Takata, R. Takahashi, J. K. Grepstad, T. Tybell, and Y. Matsumoto, *Electrochem. Solid-State Lett.*, 2012, **15**, E19–22.
18. J. A. Switzer, and G. Hodes, *MRS Bull*., 2010, **35**, 743-752.
19. Y. Yamamoto, K. Nakajima, T. Ohsawa, Y. Matsumoto, and H. Koinuma, *Jpn. J. Appl. Phys.*, 2005,Part 1 **40**, L511–514.
20. JCPDS Card No. 006-0434.
21. M. Sakurai, H. Tada, K. Saiki, and A. Koma, *Jpn. J. Appl. Phys.,* 1991, **30**, L1892-1894.
22. S. Yaginuma, K. Itaka, M. Haemori, M. Katayama, K. Ueno, T. Ohnishi, M. Lippmaa, Y. Matsumoto, and H. Koinuma, *Appl. Phys. Exp.*, **2008**, 1, 015005 (1-3).
23. C. L. Pang, R. Lindsay, and G. Thornton, *Chem. Soc. Rev.*, 2008, **37**, 2328–2353.
24. Y. Matsumoto, S. Takata, R. Tanaka, and A. Hachiya, *J. Appl. Phys.*, 2011, **109**, 014112 (1-3).
25. D. S. Boudreaux, F. Williams, and A. Nozik, *J. Appl. Phys.*, 1980, **51**, 2158–2163.
26. K Momma, and F. Izumi, *J. Appl. Crystallogr*. 2008, **41**, 653-658.